frontiers | Frontiers in Built Environment

TYPE Original Research
PUBLISHED 01 August 2024
DOI 10.3389/fbuil.2024.1463682

OPEN ACCESS

EDITED BY
Gen-Shu Tong,
Zhejiang University, China

REVIEWED BY
Chao-Qun Yu,
Zhejiang University, China
Nan-ting Yu,
Zhejiang University of Technology, China
Chao Hou,
Southern University of Science and Technology, China

*CORRESPONDENCE
Ruming Feng,
fengrm@hhwlab.com

RECEIVED 12 July 2024
ACCEPTED 17 July 2024
PUBLISHED 01 August 2024

CITATION
Li G, Pan T, Feng R and Zhu L (2024), Reliability analysis of mooring chains for floating offshore wind turbines.
Front. Built Environ. 10:1463682.
doi: 10.3389/fbuil.2024.1463682

Reliability analysis of mooring chains for floating offshore wind turbines

Guangming Li, Tianguo Pan, Ruming Feng* and Liyun Zhu

Red Bay Laboratory, Shanwei, China

As offshore wind farms move into deeper waters, around 80 m, the high costs necessitate replacing bottom-fixed turbines with floating offshore wind turbines, which require mooring systems to maintain stability within design limits. Data from previous projects in China indicate that mooring systems can constitute about 20% of the total investment. Thus, reducing mooring system costs can significantly benefit the development of next-generation floating wind farms. This paper discusses the reliability analysis of mooring chains for floating wind turbines to optimize inspection plans and strategies, thereby saving on maintenance costs over their design lifetime. A case study on S-N curve based fatigue reliability analysis is conducted using both Monte Carlo Simulation and First Order Reliability Method (FORM), with consistent results from both methods. Additionally, three sensitivity analysis cases identify key parameters for the fatigue reliability analysis.

KEYWORDS

reliability analysis, Monte Carlo simulation, offshore mooring chain, first order, reliability method

1 Introduction

Recently, offshore wind power has drawn more attention due to its intrinsic advantages. One of the primary advantages is the better quality of the wind resources in offshore locations, where the wind speed is usually greater and steadier (Hong et al., 2015; Dong and Yuan, 2023; Xiang et al., 2023). As offshore wind farms enter into deeper waters, especially for those deeper than 80 m, the traditional bottom-fixed offshore wind turbines such as mono-piles, tripods, or jackets will lose economic advantages. A new concept of floating offshore wind turbine (FOWT) becomes a more feasible and cost-saving solution. Generally, FOWTs can be categorized into four different types, i.e., the SPAR type, the semi-submersible type, the TLP type, and the barge type (Jonkman, 2009).

For FOWTs, the mooring system is one of the most important systems, accounting for approximately 20% of the total project investment. Therefore, the design and maintenance of the mooring systems for FOWTs play an important role in minimizing the total cost. The mooring system design requires a large number of design cycles with the satisfaction of the complex design constraints to achieve an economically competitive solution (Heyl and Duggal, 2009). An optimized mooring design shall keep both the translational and rotational motion of an FOWT within acceptable limits. To save design costs, a Harmony Search based mooring optimization program has been applied to study an optimum cost as a function of safety factor and required maximum offset of the offshore

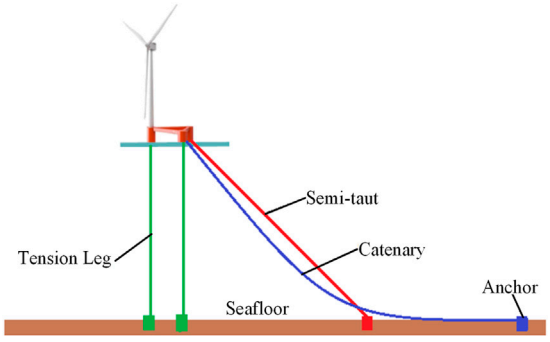

FIGURE 1
Schematic of typical mooring categories for a FOWT.

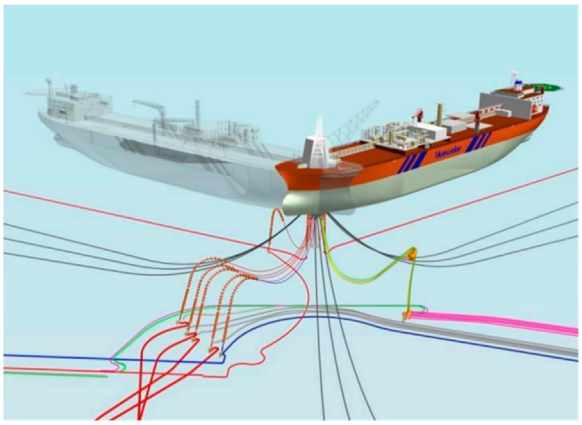

FIGURE 2
Single point mooring system.

floating structure by finding anchor leg component size and declination angle (Ryu et al., 2007).

For FOWTs, there are usually four categories of mooring systems. First, a catenary mooring system is, by far, the most widely used due to its simple design and installation. The restoring force of the FOWT is mainly provided by the self-weight of the catenary chain. The main drawback of this mooring type lies in its large footprint. Second, a semi-taut mooring system, see Figure 1, can reduce the total length of the mooring lines and footprint, the restoring force of which depends on the stretching of the line material. Nevertheless, this type has an inclination angle with the seabed, which can exert an uplift force on the anchor foundation. The Single Point Mooring (SPM) system, as a third category see Figure 2, is suitable for ship-shaped floaters, of which the mooring line top ends are fastened to a tower or turret with bearings to allow the floater weather-vane freely to minimize the environmental loads. The fourth type of mooring system is tension-legs, which is suitable for the TLP-type FOWT. Compared to the SPAR- or SEMI-type FOWT, the TLP-type FOWT tends to be lighter, smaller, and more stable, especially in harsh environments. However, the investment cost of the tension-leg mooring system is much higher than the former ones.

Permanent mooring systems shall be designed to remain offshore for decades and unable to be sheltered no matter how catastrophic the storms encountered are during operation. Hence, these mooring systems are designed with adequate capacity to withstand all design extreme conditions, which consist of the ULS, ALS, and FLS according to DNVGL-OS-E301 (DNVGL-OS-E301, 2015). Although great attention has been paid to permanent mooring design, it has been reported that there are failure accidents of offshore moorings from time to time, with an approximate failure probability on an order of 1.0×10^{-3}. Previous industry experience shows the primary reason for mooring line failure is the deterioration of the line components over time, i.e., corrosion-induced or fatigue-induced. As is known, the consequences of a mooring line failure may include risk to personnel, damage to dynamic cables, collisions with adjacent FOWTs and subsea infrastructures, repair or replacement costs, production loss, and even public reputation damage. Therefore, cost-effective and efficient inspection and monitoring programs, for the mooring system of FOWTs, shall be developed to detect any potential degradation or deterioration early enough to prevent a significant economic loss.

For the development of FOWTs in China, there are several demonstration application projects in the industry so far. Most of the projects have chosen a 3×3 whole catenary chain solution for the station-keeping system. As is known to all, offshore mooring chains have been widely used for many years, no matter for temporary or permanent mooring systems in the offshore industry. Two types of chain links, i.e., stud and studless as shown in Figure 3, are widely used for offshore mooring applications. Stud chain links are preferable for temporary mooring lines, while studless chains are more common for permanent moorings. The reasons for the wide application of chain links lie in their easier handling and installation, torsional free properties, and high resistance to wear and abrasion when in contact with other interfaces. The available steel grades for offshore moorings are R3, R3S, R4, R4S, R5, and R6 with increasing tensile strength. Therefore, this paper focuses mainly on the reliability and integrity management of mooring chains for FOWTs.

The main damage and degradation mechanisms, for a chain-made mooring line, include corrosion, wear, and fatigue, which are always present and unavoidable, especially in offshore environments. Steel structures are often affected by corrosion during use (Tong et al., 2023; Zhu et al., 2023; Duan et al., 2024; Wu et al., 2024; Yu et al., 2024). The corrosion of chain links, see Figure 4, is defined as a material loss due to an electrochemical attack by ambient surroundings. The corrosion rate is highly dependent on the ambient water temperature, marine growth, flow velocity, oxygen content, microbiological beings attacks, etc. The wear of the chain is defined as a progressive loss of material on surfaces due to relative motion between adjoining links. The wear rate depends on the axial line load and the number of rotation cycles between consecutive links. Hence, the mooring chain is usually protected against corrosion and wear using appropriate coatings. Moreover, fatigue is a degradation process for mooring chains due to cyclic loads over a long period which can gradually reduce the strength of the material and eventually trigger a failure. Usually, there are three stages for a fatigue-induced failure, i.e., crack initiation, steady crack propagation, and rapid crack propagation (Chen et al., 2024).

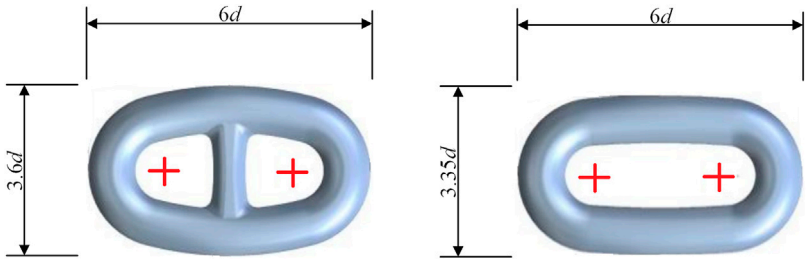

FIGURE 3
Stud chain link (left) and studless chain link (right).

FIGURE 4
The general and pitting corrosion of mooring chains (Mendoza et al., 2022).

An integrity management program shall be developed to ensure that the mooring system can fulfill its function requirement during the design lifetime with controlled deterioration rates. According to API RP 2I, the need for a rigorous, effective inspection of mooring hardware is apparent because most of the mooring failures involved faulty mooring components including corroded or physically damaged wire-rope or chain, or mooring hardware of inferior quality. This recommended practice gives good detail on how to perform inspections for mooring line components (API RP 2I, 2008). Based on in-service inspection data, the reliability analysis is an effective method to assess the failure probability of each mooring component, which can be combined to calculate the risk of the whole mooring line or system. The risk can be of great help in developing the mooring component discard criteria or an optimized mooring inspection frequency and strategy to save maintenance costs. For the mooring system of FOWTs, an in-service inspection plan shall be developed after the installation based on an assumed deterioration rate throughout its service lifetime. Developing a comprehensive and well-optimized in-service inspection plan is quite challenging and there is always room for improvements. For a well-developed in-service inspection plan, not only the obvious degradations such as general corrosion, pitting corrosion, and excessive abrasion, but also the smaller-sized defects such as fatigue cracks, and wire strand breaks can be identified and located. Based on the periodical inspection results, some unexpected anomalies or degradation rates may be identified. Under this circumstance, a reliability assessment can be performed to determine whether the initial in-service inspection plan shall be updated or adjusted to address newly identified anomalies to achieve consistent integrity for the whole mooring system during its service lifetime.

Structural reliability analysis can directly quantify how uncertainties in input parameters can affect the structural response. A large amount of previous research has been done for the development of structural reliability analysis methods. Early work on the reliability theories mainly consists of (Cornell, 1968; Hasofer and Lind, 1974). The first-order second moment (FOSM) theories are an early simplified method for reliability analysis (Ang and Tang, 1984; Madsen et al., 1986; Ditlevsen and Madsen, 1996; Nowak and Collins, 2012). For FOSM, each random variable is depicted by only the mean and the variance for reliability calculation. Later on, a joint probability distribution of all uncertain random variables is introduced, and the probability of failure can be integrated directly concerning the limit state function on the failure domain. For this level of reliability analysis, the approximate simulation methods, such as first order reliability method (FORM) (Zhao and Ono, 1999; Melchers and Andre, 2018; Zhao et al., 2020) and second order reliability method (SORM) (Huang et al., 2018; Rackwitz, 2001), together with more advanced techniques such as Monte Carlo Simulation (MCS) (Cardoso et al., 2008; Zhang et al., 2010) and Importance Sampling Methods (ISM) (Zhang, 2012; Shayanfar et al., 2018) are widely used worldwide. Among these, the algorithm of MCS is straightforward and suitable for highly nonlinear limit state function problems. The accuracy of an MCS analysis is mainly dependent on the total number of sample points. If the failure probability is on an order of 1×10^{-3}, then the total sample points shall be on an order of 1.0×10^{5} to obtain satisfactory accuracy. Later on, the response surface method (RSM) was developed for the structural reliability analysis when the limit state function has no closed form. In this method, a transfer function correlates the input parameters to the structural response which can be obtained approximately in terms of the response surface function. The work of (Bucher and Bourgund, 1990; Rajashekhar and Ellingwood, 1993) laid a foundation for RSM, further developed by (Zheng and Das, 2000; Yu et al., 2002).

For decades, reliability-based and risk-based approaches have been widely employed for developing and optimizing the inspection plans for offshore structures, to list just a few of them (Madsen et al., 1990; Moan et al., 2000; Faber, 2002; Goyet et al., 2002; Straub and Faber, 2006; Rezende et al., 2024). The Bayesian decision theory has

been adopted to minimize the overall maintenance costs including costs of failures, repairs, and inspections. Based on structural reliability analysis, the risk-based inspection plan can also be developed for offshore structural components subject to fatigue damage, see work of (Fujita et al., 1990; Moan and Song, 2000; Li and Zou, 2024; Meng et al., 2024; Oyegbile and Muskulus, 2024).

Recent research on the analysis of offshore mooring chains is relatively limited. Bergara et al. (Bergara et al., 2022) have adopted analytical, numerical, and experimental methods to assess fatigue crack propagation in offshore mooring chains under service conditions. Peunte et al. (Peunte et al., 2024) evaluate various spectral fatigue assessment methods for estimating damage caused by stress loads for offshore mooring systems and dynamic cables. Zhao et al. (Zhao et al., 2023) analyzed the system reliability of the mooring system for a floating offshore wind turbine based on an environmental contour approach.

This paper focuses on the reliability analysis of the offshore mooring chains for FOWTs. The methodology on formulating the limit state functions for chain strength and fatigue failure modes is presented, followed by the numerical simulation algorithm of FORM to solve the reliability index and probability of failure. A detailed case study is performed on *S-N* curve based fatigue reliability analysis, coupled with a parametric study to identify the dominant parameters of the fatigue reliability analysis.

2 Methodology on chain reliability analysis

A typical offshore mooring system for a FOWT consists of mooring line segments, connectors, anchor foundation, chain jack, chain stop, fairlead, etc. Data from recognized international standards shows that the anchor foundations and connectors typically have much higher reliability on strength and fatigue than mooring line segments made of chain links. Hence, this study focuses on the mooring chain reliability analysis for FOWTs.

The reliability analysis of offshore mooring chains shall consider both the ultimate and fatigue limit states. As mentioned in the introduction section, the failure modes for offshore mooring chains mainly consist of general corrosion, wear, and fatigue. The results of mooring chain reliability analysis can be directly incorporated into a risk-based inspection plan, which is by far the most effective method for developing the in-service inspection plan for offshore structures. The advantage of employing a risk-based inspection method for developing the in-service inspection plan lies in that the new condition data collected by periodical inspections can be timely incorporated to update and optimize the in-service inspection plan for the future.

Typically, there are four major steps for reliability analysis of offshore mooring chains: 1) Select an appropriate target reliability level based on the consequence of failure; 2) Formulate the limit state function of each failure mode and identify the random variables in the function; 3) Specify the distribution types and the statistical parameters, such as the mean value and COV, for all the random variables involved; 4) Compute the reliability of the mooring chain for the considered failure mode.

The ultimate limit state function for the structural reliability of a mooring line can be defined by Eq. 1. The probability of failure of the mooring line can be computed by Eq. 2.

$$g = R - (S_p + S_e) \tag{1}$$

where R denotes the mooring line strength resistance, S_p denotes the mooring line pre-tension, and S_e denotes the extreme mooring line tension under extreme storm conditions.

$$P_f = P(g \le 0) = P\left[R - \{X_p S_p + X_e S_e(t)\} \le 0\right] \quad t \in [0, T] \tag{2}$$

where R is the line resistance, t is the time period considered, usually in years, X_p denotes a model uncertainty factor considering the possible variation of the nominal pre-tension of the mooring line, S_p can be taken as the deterministic pre-tension of the mooring line by design, X_e denotes a model uncertainty parameter for the evaluation of the extreme mooring line tension, and $S_e(t)$ denotes the extreme mooring line tension at the considered time period of t (yrs).

For the fatigue reliability analysis of mooring chains of FOWTs, both the *T-N* curve based, *S-N* curved based, or fracture mechanics based fatigue reliability analyses can be chosen. Compared to the third fracture mechanics method, the former two are relatively well-developed and straightforward to implement. A drawback of the *T-N* curve based or *S-N* curve based method is that the fatigue reliability cannot be updated according to the new condition data collected during the in-service inspection. If this issue has to be considered, the fracture mechanics based reliability analysis must be chosen.

For the *S-N* curve based fatigue reliability analysis, the Miner-Palmgren model (Miner, 1945) is adopted to formulate the limit state function. Based on Miner's rule, the fatigue damage $_D$ can be computed by Eq. 3. Let $f(s)$ be the probability density function of the stress range in mooring chains under considered sea states. The total fatigue damage to chain links can be estimated by Eq. 4.

$$D = \sum_{i=1}^{N_s} \frac{n_i}{N_i} \tag{3}$$

where n_i is the number of stress cycles in i^{th} sea-state, N_i is the number of cycles to cause the fatigue crack under a constant stress amplitude for i^{th} sea-state, and Ns is the total number of sea-states considered.

$$D \approx n \int_0^\infty \frac{f(s)ds}{N(s)} = \frac{n}{K} \int_0^\infty s^m f(s)ds = \frac{n}{K} E(s^m) \tag{4}$$

where n is the total number of stress cycles for a considered time period, K is the intercept of the *S-N* curve, m is the slope of the SN curve, and $E(s^m)$ is the expected value of the random stress-range distribution to the power of m.

Therefore, the limit-state function for the *S-N* curve based fatigue reliability analysis can be formulated by Eq. 5. Similarly, the limit state function for the *T-N* curve based fatigue reliability can be formulated by Eq. 6. For a narrow-banded Gaussian process, the stress range peaks follow a Rayleigh distribution. The mean value of the tension range for a short-term sea state can be estimated by Eq. 7.

$$g = \Delta - \frac{n}{K} E(s^m) \tag{5}$$

where Δ is the fatigue resistance, usually taken as 1.

$$g = \Delta - \frac{n}{K} E(R^m) \tag{6}$$

where R denotes the ratio of the tension range of the mooring line to nominal breaking strength.

$$E(R^{m}) = \left(\sqrt{2}\,R_{\sigma}\right)^{m}\Gamma\left(1+\frac{m}{2}\right) \tag{7}$$

where R_σ is the standard deviation of the combined low and wave frequency tension range, and $\Gamma(\bullet)$ denotes the gamma function.

Therefore, for a short-term sea state, the *T-N* curve based fatigue limit stat function can be eventually written as Eq. 8. However, the wave-induced long-term stress range response of offshore structures follows a Weibull distribution. The expected value of the m^{th} order of the stress range can be approximated by Eq. 9. Hence for a long-term sea state, the *S-N* curve based fatigue limit stat function can be written as Eq. 10.

$$g = \Delta - \frac{n}{K}\left(\sqrt{2}\,R_{\sigma}\right)^{m}\Gamma\left(1+\frac{m}{2}\right) \tag{8}$$

$$E(s^{m}) = A^{m}\Gamma\left(1+\frac{m}{B}\right) \tag{9}$$

$$g = \Delta - \frac{vT}{K}X_{w}{}^{m}A^{m}\Gamma\left(1+\frac{m}{B}\right) \tag{10}$$

where v is the number of stress cycles per year on average, T is the time period considered, X_w is a model uncertainty coefficient for wave loading estimation, A and B are the Weibull distribution parameters respectively, and m and K are the *S-N* curve related parameters respectively.

As for the fracture mechanics based fatigue reliability analysis, the crack growth can be formulated by using Paris Law (Paris and Erdogan, 1963) as follows:

$$\frac{da}{dN} = C(\Delta K)^{m} \tag{11}$$

where a is the crack depth in chain links, N is the number of stress cycles, C and m are crack growth parameters of the chain material, and ΔK is the stress intensity factor range, which can be calculated by Eq. 12.

$$\Delta K = S\cdot Y(a)\cdot\sqrt{\pi a} \tag{12}$$

where Y(a) is the geometry function of the crack. Combining Eq. 11, 12, and doing an integration from the initial crack depth a_0 to the final crack depth a_c, Eq. 13 can be obtained.

$$\int_{a_0}^{a_c}\frac{da}{\left(Y(a)\sqrt{\pi a}\right)^{m}} = n\cdot C\cdot E[S^{m}] \tag{13}$$

For a long-term sea state, the fracture mechanics based fatigue limit stat function can be eventually formulated as Eq. 14. After the formulation of the limit state functions for different failure modes of mooring chains, the FORM, SORM, or MCS numerical methods can be used to compute the probability of failure P_f and the reliability index β.

$$g(T) = \int_{a_0}^{a_c}\frac{da}{\left(X_Y Y(a)\sqrt{\pi a}\right)^{m}} - vT\cdot C\cdot X_{w}{}^{m}A^{m}\Gamma\left(1+\frac{m}{B}\right) \tag{14}$$

where a_0 is the initial crack depth, a_c is the final crack depth, v is the number of stress cycles per year on average, T is the time period considered, X_w and X_Y are the model uncertainty coefficients for wave loading estimation, and geometry function calculation respectively, A and B are the Weibull distribution parameters respectively.

As is known, the offshore mooring line is a series system that may fail if any of its chain links or components fail. If considering a mooring line consists of a total of N joints or components, and assuming the events of failure for different joints are mutually independent, then the probability of failure of the mooring line can be computed by Eq. 15. Finally, the reliability of index β_s of the mooring line can be calculated by Eq. 16.

$$P_{fs} = 1 - \prod_{i=1}^{N}(1-P_{fi}) \tag{15}$$

where P_{fs} and P_{fi} denote the system and single joint probability of failure respectively.

$$\beta_s = -\Phi^{-1}(P_{fs}) \tag{16}$$

where $\Phi^{-1}(\bullet)$ denotes the inverse of the standardized normal distribution function.

The algorithm of FORM for a reliability analysis can be summarized according to the reference (Melchers and Andre, 2018) as follows:

1) Initialize the checkpoint vector, such as $\boldsymbol{x}^{\star} = \boldsymbol{x}^{(1)} = \boldsymbol{\mu}_X$, and let iteration step m = 1.
2) Use Rosenblatt or Nataf transformation to transform all basic random variables to standard Normal distributed random variables, $y_i^{(m)} = \Phi^{-1}[F_i(x_i{}^{(m)})]$ $(i = 1, 2, \ldots, n)$.
3) Transform the limit state function from **X**-space to standardized normal Y-space by $\boldsymbol{g}(\boldsymbol{x}) = \boldsymbol{g}(\boldsymbol{y})|\boldsymbol{J}|$, where $\boldsymbol{J}$ is the Jacobian Transformation Matrix.
4) Use the relations of $\boldsymbol{g}_y{}^{(m)} = [\boldsymbol{J}]^{-1}\boldsymbol{g}_X{}^{(m)}$ and $\boldsymbol{\alpha}^{(m)} = \boldsymbol{g}_y{}^{(m)}/\sqrt{\boldsymbol{g}_y(m)\mathrm{T}\cdot\boldsymbol{g}_y{}^{(m)}}$ to compute the direction cosines $\boldsymbol{\alpha}^{(m)}$ and $\boldsymbol{g}(\boldsymbol{y}^{(m)})$, the current step reliability index can be computed by $\boldsymbol{\beta}^{(m)} = -\mathbf{y}(m)\mathrm{T}\cdot\boldsymbol{\alpha}^{(m)}$, where the gradient vectors can be calculated by $\boldsymbol{g}_X{}^{(m)} = \partial g^{(m)}/\partial x_i$, $\boldsymbol{g}_y{}^{(m)} = \partial g^{(m)}/\partial y_i$ $(i = 1, 2, 3, \ldots, n)$.
5) A new iteration point can be updated by $\boldsymbol{y}^{(m+1)} = -\boldsymbol{\alpha}^{(m)}\left[\beta^{(m)} + \frac{g(\boldsymbol{y}^{(m)})}{[\boldsymbol{g}_y{}^{(m)}\boldsymbol{g}_y{}^{(m)}\mathrm{T}]^{\frac{1}{2}}}\right]$.
6) Use an inverse transformation relationship $x_i{}^{(m+1)} = F_i^{-1}[\Phi(y_i{}^{(m+1)})]$ $(i = 1, 2, \ldots, n)$ to get the new iteration point in X-space.
7) Update the iteration step by $m = m + 1$, repeat the iteration procedure from step2 to step6 until the reliability index $\beta^{(m)}$ stabilize in value.

3 Case study analysis

Now a case study is performed concerning the *S-N* curve based fatigue reliability analysis, the limit state function of which is Eq. 10. Both the FORM and MCS methods are employed for the computation of the probability of failure and the reliability index. For the case study, a total of five random variables are identified in the limit state function, i.e., the fatigue resistance Δ, the intercept of the *S-N* curve K, the model uncertainty factor for wave loading estimation X_w, and two Weibull distribution related parameters A and B. The distribution of these random variables and their statistical parameters are assumed and summarized in Table 1 below.

TABLE 1 The assumed distribution and statistical parameters of the random variables.

Random variables	Symbol	Distribution	Mean value	COV (%)
Fatigue resistance	Δ	Normal	1.0	20.0
Intercept of SN curve	$\log_{10}(K)$	Log-normal	12.6	1.7
Model uncertainty factor for wave	X_w	Log-normal	1.0	18.0
Weibull distribution parameter	$\ln(A)$	Normal	2.3	7.0
Weibull distribution parameter	$1/B$	Normal	1.4	7.0

To perform the *S-N* curve based fatigue reliability analysis by using the FORM method, the basic random variables should all be transformed into a Normal distribution $\boldsymbol{X}$ space by redefining the involved random variables as Eq. 17. An equivalent limit station function to Eq. 10, in the Normal distribution space, can be expressed as Eq. 18.

$$X_1 = \Delta, X_2 = \ln(\log_{10} K), X_3 = \ln(X_w), X_4 = \ln(A), X_5 = 1/B \tag{17}$$

$$g(X) = X_1 - \nu T \cdot 10^{-e^{X_2}} \cdot e^{mX_3} \cdot e^{mX_4} \Gamma(1 + mX_5) \tag{18}$$

$$Y_i = \frac{X_i - \mu_{X_i}}{\sigma_{X_i}} \quad (i = 1, 2, \ldots, 5) \tag{19}$$

By coupling a new transformation of Eq. 19, the equivalent limit station function in Eq. 18 can be further transformed into a standardized Normal distribution $\boldsymbol{Y}$ space as Eq. 20. For the FORM analysis, a key step is performing the first-order derivative of the limit state Eq. 18 concerning each basic random variable X_i as Eq. 21-1–21-6

$$G(Y) = \left(\mu_{X_1} + \sigma_{X_1} Y_1\right) - \nu T \cdot 10^{-e^{\mu_{X_2} + \sigma_{X_2} Y_2}} \cdot e^{m\left(\mu_{X_3} + \sigma_{X_3} Y_3\right)} \cdot e^{m\left(\mu_{X_4} + \sigma_{X_4} Y_4\right)} \cdot \Gamma\left[1 + m\left(\mu_{X_5} + \sigma_{X_5} Y_5\right)\right] \tag{20}$$

$$\frac{\partial G(\mathbf{X})}{\partial X_1} = 1 \tag{21-1}$$

$$\frac{\partial G(\mathbf{X})}{\partial X_2} = \nu_0 T \cdot 10^{-e^{X_2}} \ln(10) e^{X_2} \cdot e^{mX_3} e^{mX_4} \cdot \Gamma(1 + mX_5) \tag{21-2}$$

$$\frac{\partial G(\mathbf{X})}{\partial X_2} = \nu_0 T \cdot 10^{-e^{X_2}} \ln(10) e^{X_2} \cdot e^{mX_3} e^{mX_4} \cdot \Gamma(1 + mX_5) \tag{21-3}$$

$$\frac{\partial G(\mathbf{X})}{\partial X_3} = -\nu_0 T \cdot 10^{-e^{X_2}} \cdot m e^{mX_3} \cdot e^{mX_4} \cdot \Gamma(1 + mX_5) \tag{21-4}$$

$$\frac{\partial G(\mathbf{X})}{\partial X_4} = -\nu_0 T \cdot 10^{-e^{X_2}} e^{mX_3} \cdot m e^{mX_4} \cdot \Gamma(1 + mX_5) \tag{21-5}$$

$$\frac{\partial G(\mathbf{X})}{\partial X_5} = -\nu_0 T \cdot 10^{-e^{X_2}} e^{mX_3} \cdot e^{mX_4} \cdot \Gamma'(1 + mX_5) \tag{21-6}$$

In Eq. 21, the first derivative of the gamma function is quite complicated. To obtain an explicit expression of the first derivative of the gamma function, the following Laplace's approximation formula (Wang, 2016) can be employed to approximate the gamma function by omitting the higher order terms.

$$\Gamma(1 + x) = \sqrt{2\pi x}\left(\frac{x}{e}\right)^x \left(1 + \frac{1}{12x} + \ldots\right) \tag{22}$$

TABLE 2 The assumed constant parameters for the base case analysis.

Parameters	Symbol	Value
Stress cycles per year	ν	1.0×10^6 cycles/yr
Time	T	3:3:21 years
The slope of *S-N* curves	m	3

Take the first derivative of Eq. 22 for x, Eq. 23 can be obtained. By substitution of the explicit expression of the derivative of the gamma function into Eq. 21, the first derivative of the limit state function for the X_5 can be written as Eq. 24.

$$\Gamma'(1 + x) = \left(\frac{x}{e}\right)^x \left[\left(\frac{\pi}{\sqrt{2\pi x}} + \sqrt{2\pi x} \cdot ln(x)\right)\left(1 + \frac{1}{12x}\right) - \frac{\sqrt{2\pi x}}{12x^2}\right] \tag{23}$$

$$\frac{\partial G(\mathbf{X})}{\partial X_5} = -\nu_0 T \cdot 10^{-e^{X_2}} e^{mX_3} \cdot e^{mX_4} \cdot m\left(\frac{mX_5}{e}\right)^{mX_5} \cdot \left[\left(\frac{\pi}{\sqrt{2\pi m X_5}} + \sqrt{2\pi m X_5} \cdot ln(mX_5)\right)\left(1 + \frac{1}{12mX_5}\right) - \frac{\sqrt{2\pi m X_5}}{12(mX_5)^2}\right] \tag{24}$$

By using a mapping relationship as shown in Eq. 19, the first derivative $\partial G(\boldsymbol{Y})/\partial Y_i$ of the limit state Eq. 20 to the basic random variables in the standardized $\mathbf{Y}$-space can be eventually obtained. Now all the input parameters are defined for the base case analysis for the *S-N* curve based fatigue reliability analysis. In the limit state function of Eq. 10, there are a total of eight variables, five of the eight are random variables as presented in Table 1. The remaining three variables are all assumed to be constants. The values of these three parameters are assumed in Table 2 below.

After performing the analysis by using the MCS and FORM simulation method, the following results can be obtained, as shown in Table 3. From the results shown in Table 3, it can be seen that the reliability index, for the *S-N* based reliability analysis subject to a long-term sea-state, matches very well between the MCS analysis and FORM analysis. The largest relative difference between the two methods is only 1.46%. What is worth mentioning is that the CPU run time, during the simulation, for MCS analysis is much longer than that of the FORM analysis.

TABLE 3 Results summary for the base case of *S-N* curve reliability analysis.

Time (yr)	P_f - MBC ($\times 10^{-4}$)	P_f - FBC ($\times 10^{-4}$)	β - MBC	β - FBC	β - dif (%)
3	1.2	1.0	3.7	3.7	0.84
6	13.2	12.2	3.0	3.0	0.83
9	46.1	42.4	2.6	2.6	1.11
12	101.0	94.1	2.3	2.3	1.12
15	178.0	166.0	2.1	2.1	1.33
18	273.7	256.0	1.9	1.9	1.46
21	384.0	362.0	1.8	1.8	0.39

Notes: P_f is the probability of failure, MBC, is the MCS, of Base Case; FBC, is the FORM, of Base Case, β is the reliability index, dif is the relative difference, and the total number of MCS, simulation methods is 900,000.

TABLE 4 Results summary of the first sensitivity analysis.

Time (yr)	β - MC1	β - FC1	β - MC2	β - FC2	β - MC3	β - FC3
3	4.220	4.930	3.680	3.711	3.006	3.031
6	3.680	3.711	3.006	3.031	2.323	2.349
9	3.287	3.313	2.604	2.633	1.921	1.949
12	3.006	3.031	2.323	2.349	1.637	1.665
15	2.781	2.812	2.101	2.129	1.415	1.444
18	2.604	2.633	1.921	1.949	1.234	1.264
21	2.452	2.481	1.790	1.797	1.081	1.111

Notes: β is the Reliability Index, M is the MCS, analysis, F is the FORM, analysis, and C1, C2, and C3 denote the subcase C1, subcase C2, and subcase C3, respectively.

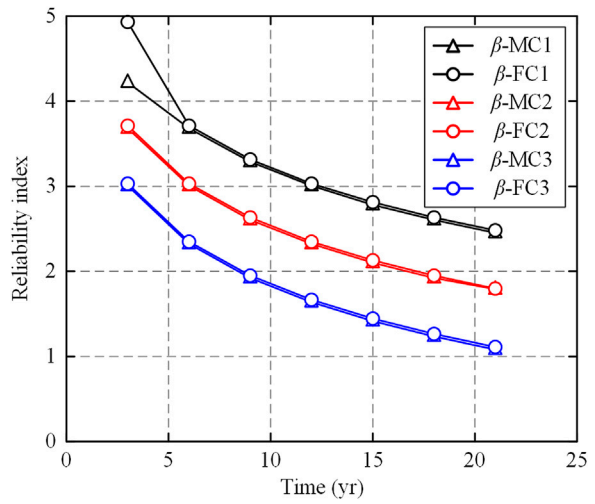

FIGURE 5
Plotting of results for the first sensitivity analysis.

4 Sensitivity analysis

A total of three sensitivity analysis cases are performed to identify the dominant parameters for the *S-N* curve based fatigue analysis. The first sensitivity analysis is on the *S-N* curve based fatigue analysis by changing the average number of stress cycles per year while keeping the remaining parameters the same as the base case. Taking $\nu = 1.0 \times 10^6$ cyc/yr as the base case (marked as Case2), the average number of stress cycles chosen for sensitivity analysis is $\nu = 0.5 \times 10^6$ cyc/yr (marked as Case1) and $\nu = 2 \times 10^6$ cyc/yr (marked as Case3) respectively. The results of this sensitivity analysis are summarized in Table 4.

Based on the data summarized in Table 4 and Figure 5 can be plotted to show the variation trends of the fatigue reliability index for both time and the sensitivity parameter. The second sensitivity analysis is on the *S-N* curve based fatigue analysis by changing the COV (Coefficient of Variation) of fatigue resistance while keeping the remaining parameters the same with the base case. Taking COV(Δ) = 20% as the base case (marked as Case6), the other two COVs of fatigue resistance chosen for sensitivity analysis are COV(Δ) = 1% (marked as Case4) and COV(Δ) = 10% (marked as Case5) respectively. The results of the second sensitivity analysis are summarized in Table 5.

Based on the data shown in Table 5, the following Figure 6 can be plotted to show the variation trend of the fatigue reliability index concerning both time and the sensitivity parameter. The third sensitivity analysis is on the *S-N* curve based fatigue analysis by changing the COV of the Weibull distribution parameters *A* and *B* while keeping the remaining parameters the same with the base case. Taking COV(*A*) = COV(*B*) = 7% as the base case (marked as Case7), the other COV values of the Weibull distribution parameters chosen for sensitivity analysis are COV(*A*) = COV(*B*) = 10% (marked as Case8) and COV(*A*) = COV(*B*) = 13% (marked as Case9)

TABLE 5 Results summary of the second sensitivity analysis.

Time (yr)	β - MC4	β - FC4	β - MC5	β - FC5	β - MC6	β - FC6
3	3.837	3.799	3.800	3.780	3.680	3.711
6	3.097	3.101	3.081	3.085	3.006	3.031
9	2.686	2.692	2.666	2.678	2.604	2.633
12	2.399	2.402	2.384	2.389	2.323	2.349
15	2.170	2.176	2.158	2.165	2.101	2.129
18	1.990	1.992	1.974	1.982	1.921	1.949
21	1.834	1.836	1.818	1.827	1.790	1.797

Notes: β is the Reliability Index, M is the MCS, analysis, F is the FORM, analysis, and C4, C5, and C6 denote the subcase C4, subcase C5, and subcase C6, respectively.

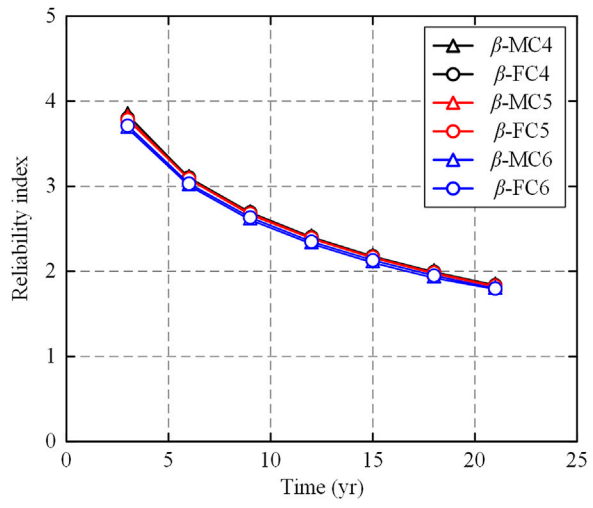

FIGURE 6
Plotting of results for the second sensitivity analysis.

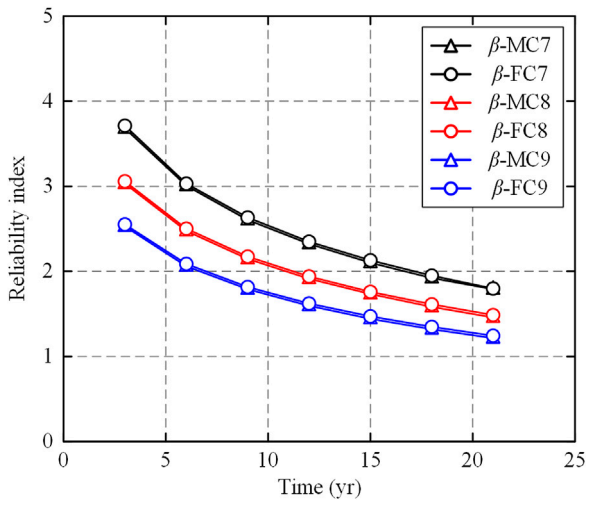

FIGURE 7
Plotting of results for the third sensitivity analysis.

TABLE 6 Results summary of the third sensitivity analysis.

Time (yr)	β - MC7	β - FC7	β - MC8	β - FC8	β - MC9	β - FC9
3	3.680	3.711	3.032	3.058	2.529	2.551
6	3.006	3.031	2.475	2.501	2.060	2.087
9	2.604	2.633	2.146	2.173	1.790	1.815
12	2.323	2.349	1.913	1.940	1.595	1.621
15	2.101	2.129	1.733	1.759	1.442	1.47
18	1.921	1.949	1.582	1.611	1.319	1.347
21	1.790	1.797	1.457	1.485	1.214	1.242

Notes: β is the Reliability Index, M is the MCS, analysis, F is the FORM, analysis, and C7, C8, and C9 denote the subcase C7, subcase C8, and subcase C9, respectively.

respectively. The results of the third sensitivity analysis are summarized in Table 6.

Based on the data shown in Table 6, the following Figure 7 can be plotted to show the variation trend of the fatigue reliability index for both time and sensitivity parameters. From the sensitivity analysis results shown in Figure 5 to Figure 7, it can be seen that the fatigue reliability indices simulated by MCS and FORM agree with each other well except for one point in Figure 5. The reason for

this mismatch point is not very clear since the FORM code for all remaining subcases works well. Possibly, for this specific subcase when compared to MCS analysis, the FORM may introduce a relatively large error when the failure probability becomes small enough. In Figure 6, the resulting plots from subcase 4 to subcase 6 almost overlap each other, which means the *S-N* curve based fatigue reliability index is not sensitive to the variation of the COV of the fatigue resistance. However, the resulting plots shown in Figure 5 and Figure 7 demonstrate that the *S-N* curve based fatigue reliability index is quite sensitive to the variation of the average number of stress range cycles per year and the COVs of the parameters in long-term Weibull distribution. Hence, more attention should be paid to these sensitive parameters for mooring chain fatigue reliability analyses in the future.

5 Conclusion

This paper addresses the reliability analyses for offshore mooring chains for FOWTs, the procedure on how to perform the reliability analysis using both the MCS and FORM is presented in great detail. The methodology on how to perform the strength and fatigue reliability of offshore mooring lines is introduced.

A case study is performed for the *S-N* curve based fatigue reliability analysis when the mooring chain link is subject to long-term sea states. Two popular numerical methods, i.e., the MCS and FORM, are employed to compute the probability of failure and reliability index. It can be seen that the fatigue reliability analysis results agree well between the two adopted methods with relative differences in fatigue reliability indices for subcases no larger than 1.46%. For the third year, the probability of failure for the *S-N* curve based fatigue reliability is relatively small, on an order of 1×10^{-4}. However, with the increase of years, the fatigue failure probability increases rapidly. After about 13 years, the fatigue probability of failure will be on an order of 1×10^{-2}. Therefore, the fatigue probability of failure for offshore mooring lines has a tight bearing on sea-state conditions and the total exposure time. What is worth mentioning is that the MCS is more time-consuming from the computational efficiency perspective. However, the derivation of the first derivative by using the FORM method is tricky and time-consuming, especially when the expression of the limit state function is complicated and highly nonlinear.

The results from the three sensitivity analysis cases demonstrate that the fatigue reliability indices are quite sensitive to the average stress cycles per year and the COVs of the Weibull distribution parameters, but not to the variation of the COV of the fatigue resistance. For the first parametric study, when the annual stress cycles change from 0.5×10^6 cyc/yr to 2×10^6 cyc/yr, the fatigue reliability indices decrease rapidly. While for the third parametric study, only a 3% COV for the Weibull distribution parameters can incur an obvious drop in the fatigue reliability indices, which indicates the *S-N* curve based fatigue reliability analysis is significantly sensitive to the parameters of the Weibull distribution. Therefore, accurate predictions of the annual stress cycles and the Weibull distribution parameters will dramatically improve the prediction accuracy of the *S-N* curve based fatigue reliability index.

Data availability statement

The original contributions presented in the study are included in the article/Supplementary Material, further inquiries can be directed to the corresponding author.

Author contributions

GL: Conceptualization, Data curation, Investigation, Methodology, Writing–original draft, Writing–review and editing. TP: Investigation, Software, Writing–original draft. RF: Conceptualization, Data curation, Investigation, Writing–review and editing, LZ: Methodology, Visualization, Writing–review and editing.

Funding

The author(s) declare that no financial support was received for the research, authorship, and/or publication of this article.

Conflict of interest

The authors declare that the research was conducted in the absence of any commercial or financial relationships that could be construed as a potential conflict of interest.

Publisher's note

References

Ang, A., and Tang, W. (1984). *Probability concept in engineering planning and design*. New York: Wiley.

API RP 2I (2008). *In-service inspection of mooring hardware for floating structures*. API.

Bergara, A., Arredondo, A., Altuzarra, J., and Martinez-Esnaola, J. (2022). Fatigue crack propagation analysis in offshore mooring chains and the influence of manufacturing residual stresses. *Ocean. Eng.* 257, 111605. doi:10.1016/j.oceaneng.2022.111605

Bucher, C., and Bourgund, U. (1990). A fast and efficient response surface approach for structural reliability problems. *Struct. Saf.* 7 (1), 57–66. doi:10.1016/0167-4730(90)90012-e

Cardoso, J., de Almeida, J., Dias, J., and Coelho, P. (2008). Structural reliability analysis using Monte Carlo simulation and neural networks. *Adv. Eng. Softw.* 39 (6), 505–513. doi:10.1016/j.advengsoft.2007.03.015

Chen, Y., Tong, J., Li, Q., Xu, S., and Shen, L. (2024). Application of high-performance cementitious composites in steel–concrete composite bridge deck systems: a review. *J. Intelligent Constr.* 2 (2), 9180012. doi:10.26599/jic.2024.9180012

Cornell, C. (1968). A Probability-based structural code. *J. Am. Concr. Inst.* 66 (12), 974–985.

Ditlevsen, O., and Madsen, H. (1996). *Structural reliability methods*. Chichester: John Wiley & Sons.

DNVGL-OS-E301 (2015). *Position mooring*. DNV GL.

Dong, Y., and Yuan, J. (2023). Projections of offshore wind energy and wave climate in Guangdong's nearshore area using CMIP6 simulations. *J. Intelligent Constr.* 1 (1), 9180007. doi:10.26599/jic.2023.9180007

Duan, S., Fan, S., Shu, G., Jiang, L., Tong, J., and Wu, Y. (2024). Numerical study and design of S35657 stainless steel welded stub columns. *J. Constr. Steel Res.* 214, 108473. doi:10.1016/j.jcsr.2024.108473

Faber, M. (2002). Risk-based inspection: the framework. *Struct. Eng. Int.* 12 (3), 186–195. doi:10.2749/101686602777965388

Fujita, M., Schall, G., and Rackwitz, R. (1990). "Adaptive reliability-based inspection strategies for structures subject to fatigue," in 5th international conference on structural safety and reliability, 1619–1626.

Goyet, J., Straub, D., and Faber, M. (2002). Risk-based inspection planning of offshore installations. *Struct. Eng. Int.* 12 (3), 200–208. doi:10.2749/101686602777965360

Hasofer, A., and Lind, N. (1974). Exact and invariant second-moment code format. *J. Eng. Mech. Div.* 100 (1), 111–121. doi:10.1061/jmcea3.0001848

Heyl, C., and Duggal, A. (2009). Mooring cost sensitivity study based on cost-optimum mooring design. *J. Ocean Eng. Technol.* 23 (1), 1–6.

Hong, S., Lee, I., Park, S., Lee, C., Chun, H., and Lim, H. (2015). An experimental study of the effect of mooring systems on the dynamics of a SPAR buoy-type floating offshore wind turbine. *Int. J. Nav. Archit. Ocean Eng.* 7 (3), 559–579. doi:10.1515/ijnaoe-2015-0040

Huang, X., Li, Y., Zhang, Y., and Zhang, X. (2018). A new direct second-order reliability analysis method. *Appl. Math. Model.* 55, 68–80. doi:10.1016/j.apm.2017.10.026

Jonkman, J. (2009). Dynamics of offshore floating wind turbines-model development and verification. *Wind Energy* 12 (5), 459–492. doi:10.1002/we.347

Li, L., and Zou, G. (2024). A novel computational approach for assessing system reliability and damage detection delay: application to fatigue deterioration in offshore structures. *Ocean. Eng.* 297, 117023. doi:10.1016/j.oceaneng.2024.117023

Madsen, H., Krenk, S., and Lind, N. (1986). *Methods of structural safety*. New Jersey: Prentice-Hall.

Madsen, H., Sørensen, J., and Olesen, R. (1990). "Optimal inspection planning for fatigue damage of offshore structures," in 5th international conference on structural safety and reliability, 2099–2106.

Martinez-Puente, E., Zarketa-Astigarraga, A., Martinez-Agirre, M., Zabala, A., Esnaola, J., Muñiz-Calvente, M., et al. (2024). Benchmarking of spectral methods for fatigue assessment of mooring systems and dynamic cables in offshore renewable energy technologies. *Ocean. Eng.* 308, 118311. doi:10.1016/j.oceaneng.2024.118311

Melchers, R., and Andre, T. (2018). *Structural reliability analysis and prediction*. Hoboken: Wiley.

Mendoza, J., Haagensen, P. J., and Köhler, J. (2022). Analysis of fatigue test data of retrieved mooring chain links subject to pitting corrosion. *Mar. Struct.* 81, 103119. doi:10.1016/j.marstruc.2021.103119

Meng, D., Yang, S., Yang, H., De Jesus, A., Correia, J., and Zhu, S. (2024). Intelligent-inspired framework for fatigue reliability evaluation of offshore wind turbine support structures under hybrid uncertainty. *Ocean. Eng.* 307, 118213. doi:10.1016/j.oceaneng.2024.118213

Miner, M. (1945). Cumulative damage in fatigue. *J. Appl. Mechanics-Transactions Asme.* 12 (3), A159–A164. doi:10.1115/1.4009458

Moan, T., and Song, R. (2000). Implications of inspection updating on system fatigue reliability of offshore structures. *J. Offshore Mech. Arct. Engineering-Transactions Asme* 122 (3), 173–180. doi:10.1115/1.1286601

Moan, T., Vårdal, O., and Johannesen, J. (2000). "Probabilistic inspection planning of fixed offshore structures," in 8th international conference on applications of statistics and probability, 191–200.

Nowak, A., and Collins, K. (2012). *Reliability of structures*. Boca Raton: CRC Press.

Oyegbile, A., and Muskulus, M. (2024). Enhancing fatigue reliability prediction of offshore wind turbine jacket joints through individual uncertainties for each degree of freedom of stress concentration factor. *Mar. Struct.* 96, 103634. doi:10.1016/j.marstruc.2024.103634

Paris, P., and Erdogan, F. (1963). A critical analysis of crack propagation laws. *J. Basic Eng. Basic Eng.* 85 (4), 528–533. doi:10.1115/1.3656900

Rackwitz, R. (2001). Reliability analysis - a review and some perspectives. *Struct. Saf.* 23 (4), 365–395. doi:10.1016/s0167-4730(02)00009-7

Rajashekhar, M., and Ellingwood, B. (1993). A new look at the response surface approach for reliability analysis. *Struct. Saf.* 12 (3), 205–220. doi:10.1016/0167-4730(93)90003-j

Rezende, F., Videiro, P., Sagrilo, L., and Oliveira, M. (2024). Reliability-based fatigue inspection planning for mooring chains of floating systems. *Reliab. Eng. Syst. Saf.* 242, 109775. doi:10.1016/j.ress.2023.109775

Ryu, S., Duggal, A., Heyl, C., and Geem, Z. (2007). "Mooring cost optimization via harmony search," in 26th international conference on offshore mechanics and arctic engineering, 355–362.

Shayanfar, M. A., Barkhordari, M. A., Barkhori, M., and Barkhori, M. (2018). An adaptive directional importance sampling method for structural reliability analysis. *Struct. Saf.* 70, 14–20. doi:10.1016/j.strusafe.2017.07.006

Straub, D., and Faber, M. (2006). Computational aspects of risk-based inspection planning. *Computer-Aided Civ. Infrastructure Eng.* 21 (3), 179–192. doi:10.1111/j.1467-8667.2006.00426.x

Tong, J. Z., Wu, R. M., and Wang, L. Q. (2023). Experimental and numerical investigations on seismic behavior of stiffened corrugated steel plate shear walls. *Earthq. Eng. Struct. Dyn.* 52 (12), 3551–3574. doi:10.1002/eqe.3920

Wang, W. (2016). Unified approaches to the approximations of the gamma function. *J. Number Theory.* 163, 570–595. doi:10.1016/j.jnt.2015.12.016

Wu, R., Wang, L., Tong, J., Tong, G., and Gao, W. (2024). Elastic buckling formulas of multi-stiffened corrugated steel plate shear walls. *Eng. Struct.* 300, 117218. doi:10.1016/j.engstruct.2023.117218

Xiang, Y., Lin, P., An, R., Yuan, J., Fan, Q., and Chen, X. (2023). Full participation flat closed-loop safety management method for offshore wind power construction sites. *J. Intelligent Constr.* 1 (1), 9180006. doi:10.26599/jic.2023.9180006

Yu, C., Tong, G., Tong, J., Zhang, J., Li, X., and Xu, S. (2024). Experimental and numerical study on seismic performance of L-shaped multi-cellular CFST frames. *J. Constr. Steel Res.* 213, 108360. doi:10.1016/j.jcsr.2023.108360

Yu, L., Das, P., and Zheng, Y. (2002). Stepwise response surface method and its application in reliability analysis of ship hull structure. *J. Offshore Mech. Arct. Engineering-Transactions Asme* 124, 226–230. doi:10.1115/1.1493199

Zhang, H. (2012). Interval importance sampling method for finite element-based structural reliability assessment under parameter uncertainties. *Struct. Saf.* 38, 1–10. doi:10.1016/j.strusafe.2012.01.003

Zhang, H., Mullen, R., and Muhanna, R. (2010). Interval Monte Carlo methods for structural reliability. *Struct. Saf.* 32 (3), 183–190. doi:10.1016/j.strusafe.2010.01.001

Zhao, G., Zhao, Y., and Dong, S. (2023). System reliability analysis of mooring system for floating offshore wind turbine based on environmental contour approach. *Ocean. Eng.* 285, 115157. doi:10.1016/j.oceaneng.2023.115157

Zhao, W., Chen, Y., and Liu, J. (2020). An effective first order reliability method based on Barzilai-Borwein step. *Appl. Math. Model.* 77, 1545–1563. doi:10.1016/j.apm.2019.08.026

Zhao, Y., and Ono, T. (1999). A general procedure for first/second-order reliability method (FORM/SORM). *Struct. Saf.* 21 (2), 95–112. doi:10.1016/s0167-4730(99)00008-9

Zheng, Y., and Das, P. (2000). Improved response surface method and its application to stiffened plate reliability analysis. *Eng. Struct.* 22 (5), 544–551. doi:10.1016/s0141-0296(98)00136-9

Zhu, X., Abe, H., Hayashi, D., and Tanaka, H. (2023). Behavioral characteristics of RC beams with non-uniform corrosion along the reinforcement. *J. Intelligent Constr.* 1 (3), 9180019. doi:10.26599/jic.2023.9180019